Hindawi
Advances in Civil Engineering
Volume 2022, Article ID 6756069, 11 pages
https://doi.org/10.1155/2022/6756069

Research Article

Influence of Multistage Target Temperature and Cyclic Loading/Unloading on the Permeability of Polypropylene Fiber Concrete

Peishan Cen,[1] Erjian Wei ,[2] and Kunyun Tian [3]

[1]*School of Construction Engineering, Zhengzhou Shengda University, Zhengzhou, Henan, China*
[2]*School of Resources and Environmental Engineering, Wuhan University of Science and Technology, Wuhan, Hubei, China*
[3]*School of Resource and Security Engineering, Henan University of Engineering, Zhengzhou, Henan, China*

Correspondence should be addressed to Erjian Wei; weierjian@wust.edu.cn and Kunyun Tian; tky1153@163.com

Received 15 February 2022; Revised 8 March 2022; Accepted 10 March 2022; Published 25 March 2022

Academic Editor: bing bai

Due to the combined effect of temperature and cyclic loading and unloading, the gas permeability of polypropylene fiber reinforced concrete structures changes during service. However, the current gas permeability test of polypropylene fiber reinforced concrete is based on a single influencing factor or a single test condition (monotonic loading), and the test conditions are quite different from the actual working conditions of the structure. To explore the permeability of polypropylene fiber reinforced concrete under cyclic loading and unloading under the influence of temperature, based on the stress principle that the specimen does not have structural damage and according to the steady-state equation of Darcy's law, the Cembureau method is adopted. The gas permeability of polypropylene fiber reinforced concrete under single loading and unloading and multistage cyclic loading and unloading at eight target temperatures is tested by the triaxial permeability test system. The results showed that (1) when the target temperature was $120^{\circ}C < T \leq 200^{\circ}C$ and $200^{\circ}C < T \leq 280^{\circ}C$, the fiber experienced two stages of "softening, melting-cooling recovery" and "melting and absorption," which caused damage to the matrix pore structure. The gas permeability at 200°C and 280°C was 246 times and 350 times that at 22°C, respectively. (2) The damage degree of the matrix strength structure increases during cyclic loading and unloading, and the permeability loss rate during cyclic loading and unloading is 1.24~1.57 times that of single loading and unloading. (3) The high target temperature leads to pore structure damage of the matrix, which not only affects the permeability of the matrix but also affects the strength structure of the matrix. When the stress ratio $R \geq 0.37$, the pore structure damage and the strength structure damage of the specimen are superimposed, resulting in the antipermeability effect of the specimen developing in the unfavorable direction. The test simulated the actual working conditions of polypropylene fiber reinforced concrete, providing a reference for building fire protection, seismic design or postdisaster evaluation.

1. Introduction

Concrete and naturally formed rock and soil are macroscopic combinations of discrete particles, which are all porous media. In actual working conditions, they are inevitably affected by the coupling of many factors, such as heat, water and stress. The evolution of influencing factors is closely related to the particle rearrangement [1], which has an important influence on the structural strength and stiffness. In recent years, polypropylene fiber reinforced concrete (PPFRC) has been widely used because of its low permeability at room temperature [2–4] and good fire and explosion resistance [5, 6]. However, the decrease in strength and increase in permeability after high-temperature damage have adverse effects on durability, which has attracted widespread attention. At present, research on the permeability of PPFRC mainly focuses on the load effect and high-temperature effect.

Relevant studies on the permeability of PPFRC under load show that the antipermeability effect of PPFRC comes from the crack resistance of fibers, which is mainly manifested in the inhibition of the generation and development of cracks in concrete by the bridging effect of fibers and the improvement of permeability resistance [7–9]. In 1963, Romualdi and Batson of the United States proposed the fiber crack arrest theory, also known as the fiber spacing theory. It

is believed that the existence of fibers reduces the propagation force at the crack tip and hinders the development of cracks, and this hindering effect is related to the fiber spacing; the smaller the fiber spacing is, the more obvious the hindering effect is [10–12]. The theory emphasizes the limiting effect of fiber spacing (content) on crack propagation in the matrix but ignores the composite reinforcement effect of the fiber itself, the bond strength between the fiber and matrix and the influence of fiber length on the reinforcement effect of the matrix, so it can only qualitatively explain the reinforcement principle of the fiber. On the basis of fiber crack arrest theory, the introduction of the linear elastic fracture mechanics principle and comprehensive consideration of fiber length, the self-composite effect and bond strength within the matrix are the main theoretical bases for the current study of fiber crack arrest enhancement. In recent years, it has been found that crack propagation is limited and impermeability is improved due to the presence of fiber strength and bonding force after concrete damage [13]. At the same time, in the recovery stage after the load damage of the concrete matrix, the fiber can also improve the crack recovery rate and reduce the permeability coefficient of concrete after cracking [14]. However, the greater the fiber content is, the better the crack resistance and impermeability. There is a threshold for different water cement ratio fiber contents, and the threshold range is generally 0.5 kg/m^3~1.5 kg/m^3 [7, 15–18]. In addition, the impermeability of concrete is greatly related to the load stress. In general, when the stress ratio is less than 0.5, the permeability of the matrix decreases with increasing stress. When the stress ratio exceeds its value, the matrix structure is easily damaged, and the permeability is greatly increased [19–22].

Relevant studies on the permeability of PPFRC after temperature action show that the voids and holes generated in the matrix after the "softening-cooling recovered" and "melting-absorption" of polypropylene fibers at high temperature are important reasons for the increase in permeability [23–30]. However, there are different views on the mechanism of pore formation after polypropylene fiber melting. Kalifa et al. [31] showed that polypropylene fibers were absorbed by the concrete matrix after melting through the "water drop" test, but the test results were greatly affected by the surface treatment degree of the specimen. Khoury [32] pointed out that the viscosity of polypropylene fiber after melting is very high and the molecular diameter (more than 14 nm) is much larger than the pore size of concrete silicate gel or solid-solid distance (1.8 nm) [33], and the possibility of absorption by the concrete matrix is very small. Bosnjak et al. [28] found through a heating test of PPFRC specimens that the PP fiber had no obvious change after the specimen was cooled by continuous heating for 20 min, and the PP fiber was absorbed after continuous heating for 6 h and 2 d. The longer the heating time was, the more obvious the absorption effect was. In addition, the free water and the bound water in the matrix have complex transformation effects at different temperatures [34]. The water loss of concrete materials under the influence of high temperature [35, 36] will lead to changes in pore structure and size as well as the generation of microcracks [37] and adversely affect the permeability resistance of concrete [38].

The above research explains the action mechanism of polypropylene fiber on concrete permeability under load and temperature. The research results provide an important reference for the engineering application of PPFRC and the fire prevention and seismic design of buildings. However, the above studies are based on a single influencing factor or a single test condition (monotonic loading), and concrete structures are often subjected to complex stress and multiple factors during service. For example, airport runways are subjected to the impact of aircraft landing, coastal buildings are subjected to the impact of waves, and concrete structures in earthquake-prone areas are subjected to cyclic loading and unloading and structural damage after fire. It is more realistic to study the permeability and damage mechanism of PPFRC under cyclic loading and unloading under the influence of temperature.

In view of this, the authors, on the basis of previous research, combined with the actual working conditions, made the PPFRC test block and imposed multilevel target temperatures on the test block. The three-axis permeability test system was used to measure the permeability of PPFRC during single loading and unloading and multistage cyclic loading and unloading. The evolution characteristics of the gas permeability of PPFRC under multistage target temperatures and cyclic loading and unloading conditions are studied.

2. Design of Experiments

The test was carried out by eight target temperatures and two loading and unloading methods. The test process is shown in Figure 1.

2.1. Test Raw Materials and Ratio. The ordinary Portland cement used in the test was produced by Henan Mengdian Group Cement Co., Ltd. and is labeled as P·O 42.5R. The fine aggregate is natural river sand, the fineness modulus is 2.70, and the apparent density is 2562 kg/m^3. The coarse aggregate is continuous graded gravel with a particle size of 5~20 mm and an apparent density of 2,622 kg/m^3. The test water was ordinary tap water. Polypropylene fiber used for test production was procured from Langfang Shuangyuan Energy Saving Technology Co., Ltd. The length was 15 mm, the diameter was 0.5 mm, the tensile strength was greater than 450 MPa, the melting point was 189°C, and the dosage was 0.9 kg/m^3. The PPFRC test block volume is 200 mm × 200 mm × 200 mm, and the strength grade is C30. The proportion is shown in Table 1.

2.2. Test System. The triaxial permeability test system for the test was produced by Jiangsu Tuochuang Scientific Research Instrument Co., Ltd., as shown in Figures 2 and 3, which mainly includes three system modules: a three-axis loading servo control system, gas (liquid) flow measurement system, and square block placement cavity.

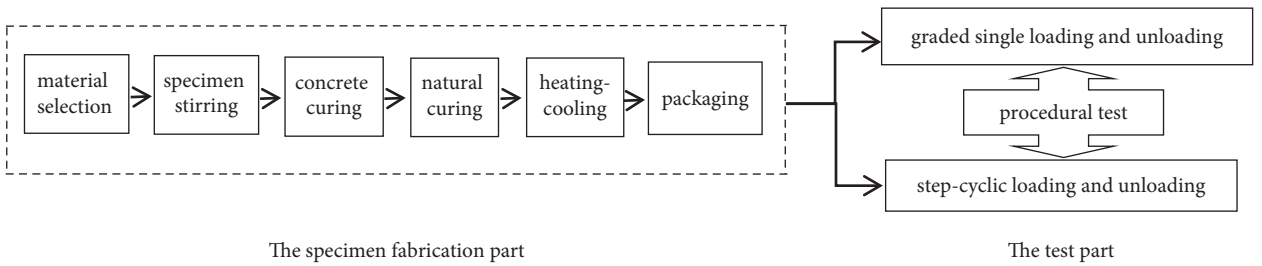

Figure 1: Test flow chart.

Table 1: PPFRC ratio table.

Strength grade	Cement (kg/m^3)	Water (kg/m^3)	Sand (kg/m^3)	Gravel (kg/m^3)	Fiber (kg/m^3)
C30	360	180	673.4	1146.6	0.9

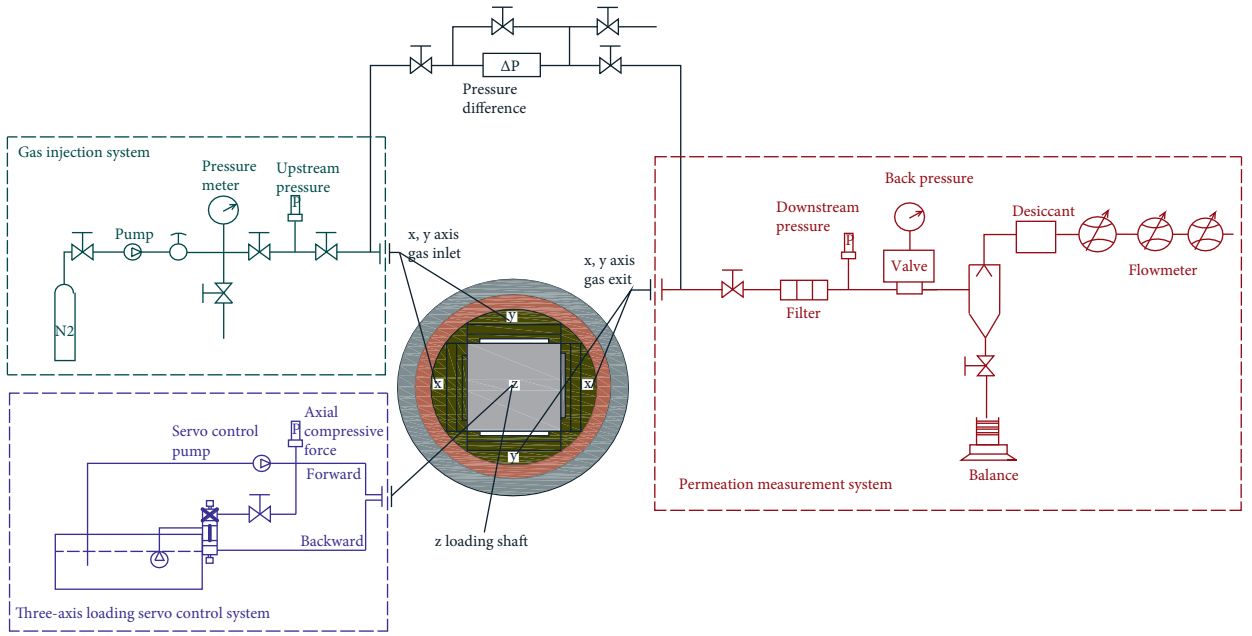

Figure 2: Structure principal diagram of the triaxial loading permeability test system.

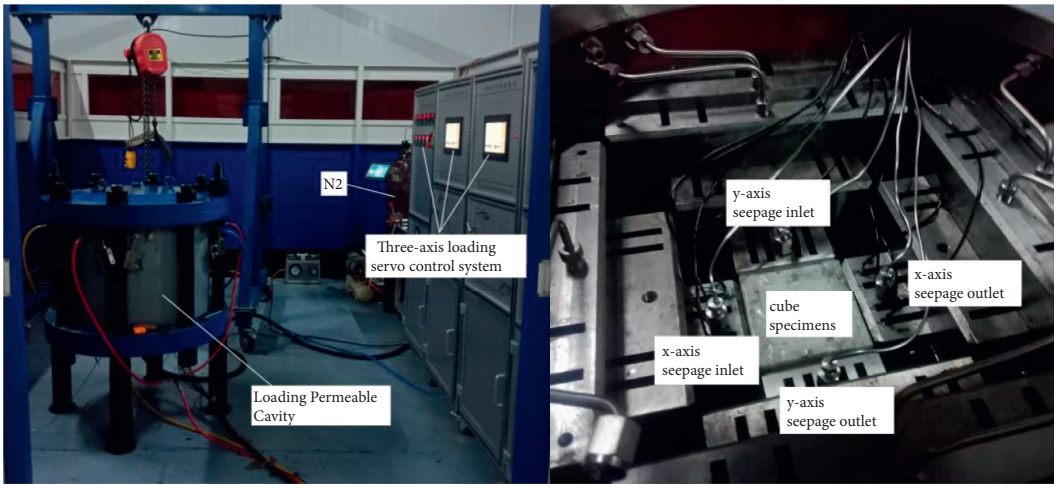

Figure 3: Triaxial loading seepage test device.

(1) Three-axis loading servo control system: piston loading, self-balancing reaction structure; three-axis independent servo system plus central digital system control, control accuracy: ≥ ±0.1% f.s. ① Three-axis loading unit: each axis contains two main loading hydraulic cylinders, with a maximum load of 1000 kN, a maximum stroke of 50 mm, and with a measurement control accuracy reaching 0.1% of the maximum force value. It can be steadily loaded for a long period. A Swiss trafag pressure sensor was used. The rated output voltage of the sensor was 2.0 mV/V ±2.5%, creep ±0.1%, nonlinearity ±0.3%, hysteresis ±0.3%, and the temperature compensation range was −10°C + 40°C. ② Servo control system: the Japanese Fuji servo control system is adopted to meet constant pressure and constant rate loading. The loading rate is 0.01~1 kN/s, maximum loading pressure is 40 MPa, control precision is 0.01 MPa, resolution ≤0.1%, and hysteresis ≤0.2%.

(2) Gas flow measurement system: the steady-state method was used to control the flow, with a pressure 0~10 MPa, and permeability coefficient measurement range 10^{-14} m^2~10^{-22} m^2. During the test, it is necessary to cooperate with the triaxial loading cylinder, encapsulate the specimen with the upper and lower pressure heads with seepage channels in the triaxial loading cylinder, and apply a certain amount of hydrostatic pressure (greater than the maximum osmotic pressure of at least 0.5 MPa) before the beginning of the permeability test to ensure that the packaging material was close to the specimen wall.

(3) Square block placement cavity: three cube specifications are 300 mm, 200 mm, and 100 mm. There are three sets of clamps, and the clamp contains the corresponding rigid cushion block, which is convenient for changing the size of the test sample; an encapsulation pressure of 0~20 MPa is used to ensure that the three axial seals are reliable.

2.3. Heating and Sealing of Specimens. The test block was made according to Table 1; the standard curing time was 28 days. At the end of the curing period, the specimens were subjected to indoor natural air drying for one month. The specimen was heated by a box-type resistance furnace, and the target temperatures were 22°C (room temperature), 40°C, 80°C, 120°C, 160°C, 200°C, 240°C and 280°C. After thermal stability for 6 h, the specimen was removed and cooled naturally to room temperature and then packaged for loading and unloading gas permeability tests. To prevent angular damage to the specimen during the loading process, the gas seepage channel is changed. The Sealing Test Specimen with Angle Copper Strip Fixed Edge Glass Adhesive is shown in Figure 4.

Figure 4: Edge angle seal of PPFRC.

2.4. Test Scheme

(1) Principle of the seepage test: the steady-state equation based on Darcy's law adopts the Cembureau method. Under a certain pressure difference on both sides of the sample, the gas permeability is related to the viscosity coefficient, flow distance and flow rate, and the permeability is calculated according to formula (1) [39].

$$K_g = \frac{2L\mu Q_0 P_0}{A\left(P_1^2 - P_2^2\right)}. \quad (1)$$

In the formula, K_g is the gas permeability of the PPFRC test block, m^2; μ is the viscosity of the test gas, S·N/m^2; Q_0 is the gas flow through the specimen, m^3/s; P_0 is atmospheric pressure under test conditions, MPa; P_1 is inlet gas pressure, MPa; P_2 is the outlet gas pressure, MPa; A is the square sample area, m^2; and L is the length of specimen, m.

(2) Test scheme: the uniaxial compression test scheme was adopted, with a confining pressure of 0, the compression axial is z-axis, and the loading and unloading rate is 0.1 kN/s. Nitrogen was selected as the permeable gas, the inlet was on one side of the x- and y-axes, the inlet pressure was 1.0 MPa, the outlet was on the other side of the x- and y-axes, and the outlet pressure was 0.5 The specimens were encapsulated by hydrostatic water with a pressure of 1.5 MPa. To ensure the permeability test effect and prevent damage to the specimen structure [40, 41], the maximum effective stress of the specimen is $0.5f_c$ (f_c is the measured peak stress of the PPFRC specimen). The test was divided into two groups, and eight specimens in each group were subjected to different target temperatures. In the first group, the specimen was subjected to 8-stage single loading, and the permeability of the specimen at each loading level was tested. After loading to $0.5f_c$, the specimen was unloaded to $0.03f_c$, and then the permeability was tested again. The second group of specimens was subjected to 8-stage cyclic loading and unloading (the permeability under load state was tested after loading the nth stage, then the permeability was unloaded to $0.03f_c$, then the permeability was tested again, and the cyclic loading and unloading was carried out successively until the 8-stage loading and unloading was

Table 2: Test results of PPFRC loading permeability under different temperatures.

State of stress	Stress ratio (R)	Permeability (kg/×10^{-17} m^2)							
		22°C	40°C	80°C	120°C	160°C	200°C	240°C	280°C
Graded cyclic loading	0.03	1.85	2.31	8.02	29.65	127.43	397.21	513.52	532.75
	0.10	1.71	2.13	7.46	27.79	119.11	373.92	491.66	512.42
	0.17	1.56	1.96	6.90	25.71	109.45	350.32	462.12	487.28
	0.23	1.41	1.78	6.35	23.68	101.04	330.75	436.64	463.87
	0.30	1.27	1.60	5.78	21.76	93.11	313.45	414.04	441.54
	0.37	1.16	1.44	5.27	19.78	86.32	298.34	403.91	433.56
	0.43	1.07	1.32	4.92	18.31	83.11	290.25	398.36	428.74
	0.50	1.01	1.26	4.77	17.65	81.71	287.27	395.82	425.74
Graded single loading	0.03	1.85	2.31	8.02	29.65	127.43	397.21	513.51	532.70
	0.10	1.69	2.10	7.41	27.38	118.11	367.92	483.66	506.42
	0.17	1.53	1.91	6.77	25.22	107.95	343.32	456.12	479.28
	0.23	1.37	1.72	6.14	23.01	99.04	319.75	428.64	453.07
	0.30	1.22	1.54	5.51	20.89	91.11	301.45	404.04	429.54
	0.37	1.08	1.37	5.00	18.87	84.32	286.34	390.01	414.56
	0.43	0.97	1.23	4.59	17.31	80.11	278.25	380.36	404.74
	0.50	0.90	1.16	4.35	16.43	76.71	271.27	371.82	397.74

Table 3: Test results of unloading permeability of PPFRC under different temperatures.

State of stress	Difference of loading-unloading stress ratio	Permeability (kg/×10^{-17} m^2)							
		22°C	40°C	80°C	120°C	160°C	200°C	240°C	280°C
Graded cyclic unloading	0.07	1.82	2.27	7.86	28.77	117.27	360.32	482.18	499.47
	0.13	1.80	2.23	7.71	28.21	114.82	350.32	470.65	486.40
	0.20	1.76	2.19	7.55	27.62	109.76	337.75	450.97	466.54
	0.27	1.73	2.14	7.35	26.72	105.07	322.20	430.51	445.58
	0.34	1.69	2.08	7.16	25.97	101.81	311.33	419.32	432.05
	0.40	1.65	2.04	6.99	25.13	99.87	302.57	402.02	416.76
	0.47	1.63	2.01	6.90	24.72	98.74	291.30	391.50	401.42
Single unloading	0.47	1.71	2.12	7.25	26.54	111.92	330.70	417.15	426.99

completed). Relevant data were automatically collected, calculated and saved in the experiment, with a data acquisition frequency of 3 seconds. Each loading and unloading stress and measurement residence time was not less than 5 min, and airflow stability was ensured for more than 3 min.

The effective stress of the specimen is calculated according to formula (2) [42], and the stress ratio is calculated according to formula (3).

$$\sigma_e = \sigma_z - \frac{1}{2}(P_1 - P_2), \tag{2}$$

$$R = \frac{\sigma_e}{f_c}. \tag{3}$$

In the formula, σ_e denotes the effective stress, MPa; σ_z is the z axial stress, MPa; R is the specimen stress ratio; and f_c is the peak stress of the specimen under uniaxial compression, MPa.

3. Experiment Results and Analysis

3.1. Test Results

(1) Test results: the test results are shown in Tables 2 and 3.

The calculation of the data in Tables 2 and 3 shows that the permeability (average) of the specimens at 200°C and 280°C is 246 and 350 times that at 22°C, respectively, indicating that the increase in temperature has a negative impact on the permeability resistance of the specimens. Under the loading conditions, the permeability of the specimen in the cyclic loading and unloading process is 1.00~1.12 times that in the single loading and unloading process, indicating that the cyclic loading and unloading conditions have a negative impact on the permeability resistance of the specimen. When the stress ratio difference is 0.47, the permeability of the specimen in the single unloading process is 1.05~1.14 times that in the cyclic loading and unloading process, indicating that the recovery degree of the specimen under single loading and unloading is higher than that under cyclic loading and unloading.

(2) R-kg curve: after fitting the stress ratio and permeability data in Table 2, the R-kg relationship curve is obtained, as shown in Figure 5.

Figure 5 shows that ① the R-kg relation curve is similar under the two stress conditions. The R-kg relation curve is steep in the early stage of loading and gentle in the later stage of loading. This indicates

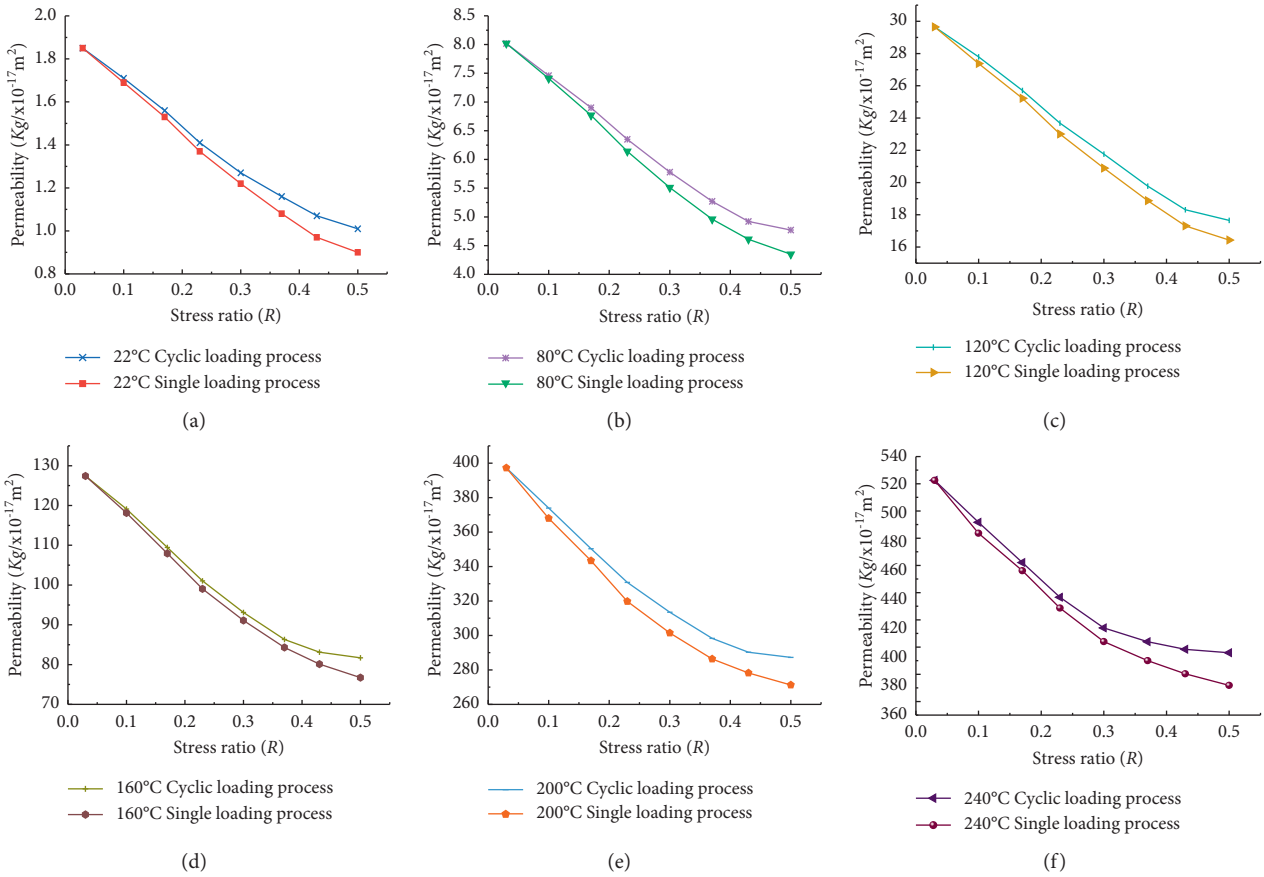

Figure 5: Evolution characteristics of the permeability of the specimen during the loading process.

that the permeability decreases significantly with increasing stress at the early stage of loading, and the stress is beneficial to the permeability resistance of the specimen. At the later stage of loading, the decline rate decreases or even remains unchanged with increasing stress. At this time, the stress develops in a disadvantageous direction to the permeability resistance of the specimen. ② With the increase in the target temperature of the specimen, the length of the linear section decreases, and the gentle section increases in the stress period. This indicates that the "window" of the stress beneficial to the impermeability of the specimen becomes narrower after the influence of high temperature, and the specimen develops in the unfavorable direction of impermeability.

(3) T-kg curve: after fitting the temperature (T) and permeability (average) in the loading process of the specimen in Table 2, the T-kg relationship curve is obtained, as shown in Figure 6.

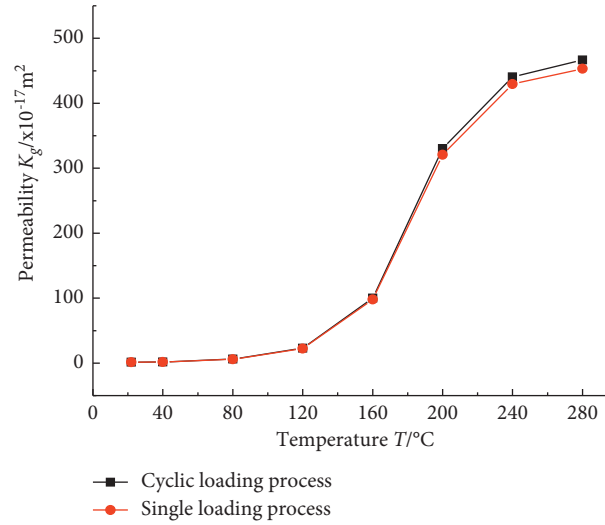

Figure 6: Evolution characteristics of permeability under temperature influence.

Figure 6 shows that, under the two stress conditions, the change in kg with increasing T experienced three stages. In the first stage, $T < 120^{\circ}C$, the T-kg linear slope is low, and the increment is small. In the second stage, $120^{\circ}C \le T \le 200^{\circ}C$, the T-kg myopia exponential function relationship, kg significantly increases. In the third stage, $200^{\circ}C < T \le 280^{\circ}C$, the increment of kg decreased, and the T-kg curve finally tended to be gentle. This shows that the temperature between 120°C~200°C has a significant impact on the seepage rate of the specimen. When the temperature is higher than 240°C, the fiber has completely melted, the total amount of cavity formed by the fiber in the matrix does not increase, and its

permeability tends to be stable, so the third stage of the T-kg curve is flat.

The above results show that the increase in target temperature and cyclic loading and unloading conditions have adverse effects on the impermeability of the specimen.

3.2. Analysis of Permeability Characteristics

3.2.1. Permeability Decline Rate. The permeability change rate is closely related to the stress conditions and temperature factors. The calculation of the permeability change rate of the specimen can intuitively reflect the influence of the two factors. The permeability parameters in Table 2 are calculated according to formula (4) to obtain the permeability decline rate of the specimen. The detailed data are shown in Table 4.

$$k_D = \frac{(k_i - k_{i+1})}{k_i} \times 100\%. \quad (4)$$

In the formula, k_D is the permeability decline rate of the specimen, %; k_i is the permeability of the specimen under stage i loading, m^2; and k_{i+1} is the permeability of the specimen under stage "$i+1$" loading, m^2.

Table 4 shows that under two stress states, k_D undergoes three stages of "Sudden Change" with temperature. The temperature ranges of the three mutations were $40^\circ C \le T \le 120^\circ C$, $120^\circ C < T \le 200^\circ C$ and $200^\circ C < T \le 280^\circ C$, and the stress ratios were 0.5, 0.43 and 0.37, respectively. It can be seen that the k_D "Sudden Change" stress ratio of the specimen moved forward with increasing temperature.

According to the literature research [7–9, 23–30] conclusions combined with the analysis of experimental results, the permeability of polypropylene fiber concrete under the influence of stress and temperature is mainly related to three factors. First are the physical bonding properties of fiber materials and concrete. Second, the damage degree of the fiber pore structure is affected by temperature. Third, the damage degree of stress affects the strength structure of the specimens.

In the first stage, the target temperature is relatively low, the thermal deformation of the polypropylene fiber is small, and the fiber is closely integrated with the matrix, as shown in Figure 7(a). The low-temperature effect causes little damage to the pore structure of the matrix, and the matrix strength of the specimen is high. At this time, the permeability is mainly dominated by pores and microcracks in the matrix. In reaction to pressure, the two produce a compression effect [22, 43], and the permeability and stress decrease linearly. Due to the good stability of the fiber and the large ductility of the matrix, when the stress continues to increase, the response time of the two to the stress is close to or reaches the limit state (large elastic-plastic deformation), and the straight line segment of the R-kg curve is longer, as shown in Figures 5(a)–5(c). Therefore, the stress value is large when the permeability is "Sudden Change."

In the second stage, the target temperature is the softening and melting stage of the polypropylene fiber. After cooling, the recovered fiber is separated from the matrix and generates voids, resulting in different degrees of damage to the pore structure of the matrix, increasing the gas permeability channel and reducing the matrix strength [28, 29], as shown in Figure 7(b). Due to the increase in the permeability channel, the matrix permeability is significantly higher than that in the first stage, as shown in Figure 6. Due to the damage to the pore structure of the matrix, the adhesion between the fiber and the matrix fades, resulting in a decrease in the strength and ductility of the matrix. When the stress response of the three is close to or reaches the limit state, the duration is shortened (the elastic-plastic deformation decreases), and the linear section of the R-kg curve is shortened, as shown in Figures 5(d) and 5(e). Therefore, the stress value decreases when the permeability is "Sudden Change."

The third stage is the high-temperature influence stage. The microstructure study shows that the polypropylene fiber disappears in the matrix after high temperatures above 200°C, and voids are formed after cooling [31, 44]. The macroscopic results of the specimen after high temperature are consistent with the microscopic results, as shown in Figure 7(c). At this time, the matrix pore structure is greatly damaged, and the strength is significantly reduced. Compared with the first three kinds of fractures, this large cavity is not sensitive to the stress response, resulting in higher permeability than the first two stages, as shown in Figure 6. Due to the large damage degree of the matrix pore structure, the fiber disappears, the matrix becomes brittle material, and the strength decreases to the minimum. In reaction to stress, the elastic-plastic deformation of the matrix is the smallest. At this time, the period of pores and voids in the matrix to reach the limit state is shortened again, and the straight line segment of the R-kg curve is shortened again, as shown in Figure 5(f). Therefore, the stress value decreases again when the permeability is "Sudden Change."

3.2.2. Permeability Loss. The permeability loss rate can reflect the damage and recovery degree of the specimen after unloading. The smaller the permeability loss rate is, the lower the damage degree of the specimen and the higher the recovery degree. According to the data in Tables 2 and 3, the permeability loss rate of the specimen during unloading is calculated according to formula (5) [45, 46].

$$k_P = \frac{(k_1 - k_{i-U1})}{k_1} \times 100\%. \quad (5)$$

In the formula, k_P is the permeability loss rate; k_1 is the permeability of the specimen under the first stage loading, m^2; and k_{i-U1} is the permeability of the specimen under unloading of level i, m^2.

The data in Table 5 show that k_P increases with increasing temperature and stress. The permeability loss rate of the loading and unloading stress ratio difference $R_D = 0.47$ was calculated. The permeability loss rate of the cyclic loading and unloading process was 1.24~1.57 times that of single loading and unloading. It can be seen that temperature rise and cyclic loading and unloading conditions have adverse effects on the impermeability of PPFRC.

Table 4: Permeability decline rate of the specimen during loading.

State of stress	Stress ratio (R)	Permeability decline rate (k_D/%)							
		22°C	40°C	80°C	120°C	160°C	200°C	240°C	280°C
Cyclic loading process	0.10	8	8	7	6	7	6	6	5
	0.17	9	8	8	7	8	6	6	5
	0.23	10	9	8	8	8	6	6	5
	0.30	10	10	9	8	8	5	5	5
	0.37	9	10	9	9	7	5	2	2
	0.43	8	8	7	7	4	3	1	1
	0.50	6	5	3	4	2	1	1	1
Single loading process	0.10	9	9	8	8	7	7	7	6
	0.17	9	9	9	8	9	7	6	5
	0.23	10	10	9	9	8	7	6	5
	0.30	11	10	10	9	8	6	6	5
	0.37	11	11	9	10	7	5	3	3
	0.43	10	10	8	8	5	3	2	2
	0.50	7	6	5	5	4	3	2	2

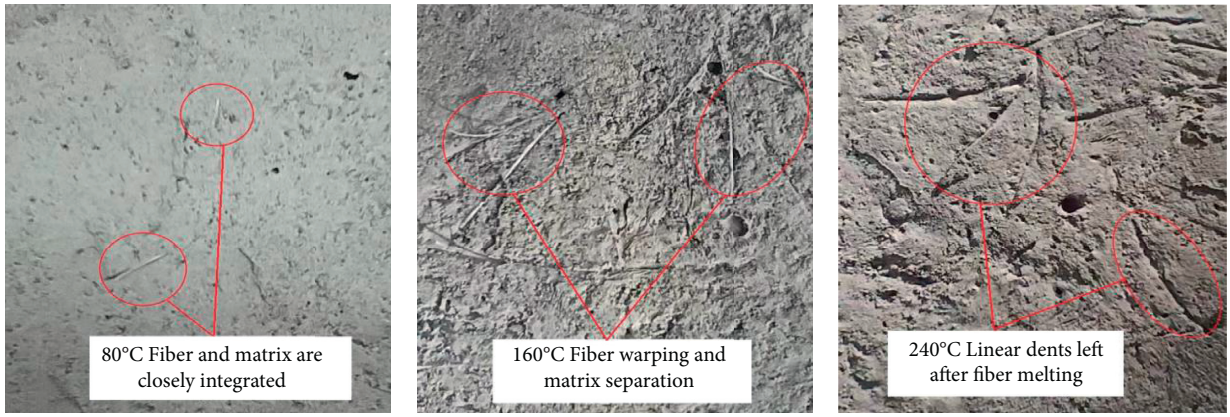

(a) (b) (c)

Figure 7: Changes in fiber in the matrix under different temperatures.

Table 5: Loss rate of unloading permeability of specimens.

State of stress	Difference of loading-unloading stress ratio (R_D)	Permeability loss rate (k_P/%)							
		22°C	40°C	80°C	120°C	160°C	200°C	240°C	280°C
Cyclic nloading process	0.07	1.62	1.73	2.00	2.97	3.43	5.23	6.10	6.25
	0.13	2.70	3.46	3.87	4.86	5.44	7.86	8.35	8.70
	0.20	4.86	5.19	5.86	6.85	9.61	11.17	12.18	12.43
	0.27	6.49	7.36	8.35	9.88	13.47	15.26	16.16	16.36
	0.34	8.65	9.96	10.72	12.41	16.16	18.12	18.34	18.90
	0.40	10.81	11.69	12.84	15.24	17.76	20.42	21.71	21.77
	0.47	11.89	12.99	13.97	16.63	18.69	23.38	23.76	24.65
Single nloading process	0.47	7.57	8.23	9.60	10.49	12.17	16.74	18.77	19.84

Note. The difference between the loading and unloading stress ratio is denoted as R_D, which is equal to the difference between the stress ratio R_i and 0.03 at stage I loading.

The analysis shows that the unloading process of the specimen is not the inverse process of loading. At the early stage of loading, the specimen is in the elastic stage. When the stress is greater than the elastic limit A, the specimen enters the plastic working stage, the closure rate of microgaps in the matrix is accelerated, and the matrix shape variable is increased. At this time, the matrix structure is partially damaged, the deformation of the specimen will not return to the original state when unloading, and there is deformation loss, as shown in Figure 8. After multistage

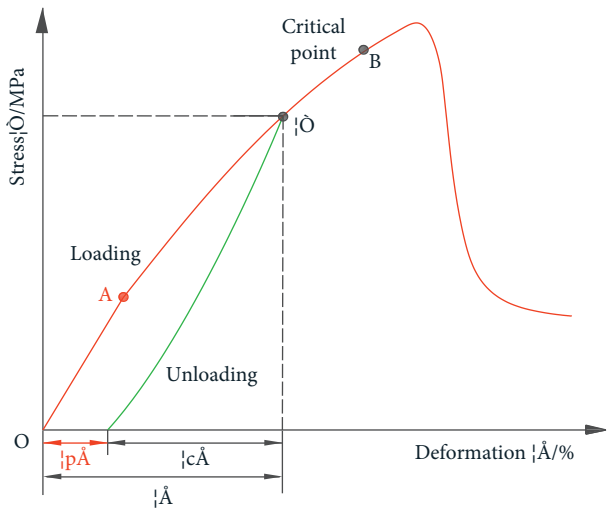

FIGURE 8: Stress-strain of the specimen during loading and unloading.

cyclic loading and unloading, the damage to the matrix strength structure increases [47], and the crack extends or increases, which adversely affects the impermeability of the specimen.

In addition, the average values of k_D and k_P of the specimens under cyclic loading and unloading conditions at $R \le 0.34$ and $T \le 120^{\circ}C$ were calculated and recorded as k_{D-LL} and k_{P-LL}, respectively. The average values of k_D and k_P of the specimens under cyclic loading and unloading conditions at $R \ge 0.37$ and $T \ge 160^{\circ}C$ were calculated and recorded as k_{D-HH} and k_{P-HH}, respectively. After comparison, it is found that the permeability decline rate of the specimen at low temperature and low stress is large ($k_{D-LL} = 8.26$), and the permeability loss rate is small ($k_{P-LL} = 4.88$). Under high temperature and high stress, the permeability decline rate of the specimen was small ($k_{D-HH} = 2.44$), and the permeability loss rate was large ($k_{P-HH} = 20.31$). The analysis shows that the high target temperature leads to damage to the matrix pore structure, which not only affects the permeability of the matrix but also affects the strength structure of the matrix. The pore structure damage and strength structure damage of the specimen are superimposed under the influence of high temperature and high stress conditions. After the superposition of the two, the failure of the pore structure accelerates the failure of the strength structure under high stress, makes the development of the matrix crack faster, and leads to the development of the matrix antipermeability effect in a disadvantageous direction.

4. Conclusions

(1) When the influence temperature of the specimen is 120°C~280°C, the fiber undergoes two stages, "softening, melting-cooling recovery" and "melting and absorption," which cause damage to the matrix pore structure. The permeability of specimens at 200°C and 280°C is 246 times and 350 times that at 22°C, respectively.

(2) Compared with single loading and unloading, cyclic loading and unloading have greater damage to the strength structure of the specimen, and the permeability loss rate of the latter is 1.24~1.57 times that of the former.

(3) After the influence of high temperature, the pore structure damage and strength structure damage of the specimen are superimposed under high stress (stress ratio is between 0.37 and 0.5). The permeability loss rate of the specimen at high temperature and high pressure is 4.16 times that at low temperature and low pressure.

(4) Although the test process simulates the working conditions of the PPFRC structure, there are still some differences between the test process and the real working conditions due to the limitations of the test equipment. For example, the difference between the heating mode of the resistance furnace and the heating mode of an open fire, as well as the difference between the independence of the heating and load processes of the specimen and the joint action of the two factors when the structure is subjected to fire, will cause changes in the permeability of the component. Therefore, the study of the permeability of components after fire or under the combined action of temperature and pressure is closer to the actual working conditions of the structure.

Data Availability

The data used to support the findings of this study are included within the article.

Conflicts of Interest

The authors declare that there are no conflicts of interest regarding the publication of this study.

Acknowledgments

The authors gratefully acknowledge the financial support from the National Natural Science Foundation of China (51604091), the Science and Technology Innovation Team Program of Henan Universities (22IRTSTHN009), and the Science and Technology Project of Henan Province for tackling key problems (222102320466).

References

[1] B. Bai, R. Zhou, G. Q. Cai, W. Hu, and G. C. Yang, "Coupled thermo-hydro-mechanical mechanism in view of the soil particle rearrangement of granular thermodynamics," *Computers and Geotechnics*, vol. 137, no. 8, Article ID 104272, 2021.

[2] C. Du, Y. S. Huang, and W. Sun, "Effect of polypropylene fiber on anti-cracking and anti-permeability properties of concrete," *Low Temperature Architecture Technology*, vol. 5, pp. 55-56, 2005.

[3] G. S. Islam and S. D. Gupta, "Evaluating plastic shrinkage and permeability of polypropylene fiber reinforced concrete,"

International Journal of Sustainable Built Environment, vol. 5, no. 2, pp. 345–354, 2016.

[4] M. Briffaut, F. Benboudjema, and L. D'Aloia, "Effect of fibres on early age cracking of concrete tunnel lining.Part I:Laboratory ring test," *Tunnelling and Underground Space Technology*, vol. 59, pp. 215–220, 2016.

[5] R. Serrano, A. Cobo, M. Isabel Prieto, and M. Nieves González, "Analysis offire resistance of concrete with polypropylene or steel fibers," *Construction and Building Materials*, vol. 122, pp. 302–309, 2016.

[6] S. M. Liu and H. Y. Hu, "Study of mechanical and resistance to chloride ion peneration properties of hybrid polypropylene fiber reinforced concrete," *Engineering Journal of Wuhan University*, vol. 52, no. 2, pp. 131–138, 2019.

[7] J. Q. Gong, W. Zheng, and W. J. Zhang, "Influence of shrinkage-reducing agent and polypropylene fiber on shrinkage of ceramsite concrete," *Construction and Building Materials*, vol. 159, pp. 155–163, 2018.

[8] M. R. Latifi, E. Biricik, and A. M. Aghabaglou, "Effect of the addition of polypropylene fiber on concrete properties," *Journal of Adhesion Science and Technology*, vol. 36, no. 4, pp. 345–369, 2022.

[9] Y. Zhang, *Study on the Mechanical Properties and Damage and Failure Morphology of Polypropylene Fiber Reinforced concrete*, Xi'an University of Technology, Xi'an, China, 2019.

[10] J. P. Romualdi and G. B. Batson, "Behavior of reinforced concrete beams with closely spaced reinforcement," *ACI Structural Journal*, vol. 60, no. 6, pp. 775–789, 1963.

[11] J. P. Romualdi and G. B. Batson, "Mechanics of crack arrestin concrete," *Journal of the Engineering Mechanics Division*, vol. 89, no. 3, pp. 147–168, 1963.

[12] J. P. Romualdi and J. A. Mandel, "Tensile strength of concrete affected by uniformly distributed and closely spaced short lengths of wire reinforcement," *ACI Structural Journal*, vol. 61, no. 6, pp. 27–37, 1964.

[13] M. H. Duan, Y. Qin, Z. G. Xu, and W. L. Ma, "Effect of polypropylene fiber on the damage and permeability of concrete," *Acta Materiae Compositae Sinica*, vol. 38, no. 10, pp. 3474–3483, 2021.

[14] A. Ding, Q. Wang, and Y. Ibrahim, "Effects of polypropylene fiber content on strength and workability properties of concrete," *Acta Materiae Compositae Sinica*, vol. 34, no. 8, pp. 1853–1861, 2017.

[15] A. N. Ede and A. O. Ige, "Optimal polypropylene fiber content for improved compressive and flexural strength of concrete," *IOSR Journal of Mechanical and Civil Engineering*, vol. 11, no. 3, pp. 129–135, 2014.

[16] O. Karahan and C. D. Atiş, "The durability properties of polypropylene fiber reinforced fly ash concrete," *Materials & Design*, vol. 32, no. 2, pp. 1044–1049, 2011.

[17] H. Hasan, N. Maroof, and Y. Ibrahim, "Effects of polypropylene fiber content on strength and workability properties of concrete," *Polytechnic Journal*, vol. 9, no. 1, pp. 7–12, 2019.

[18] K. R. Akça, Ö. Çakır, and İ. Metin, "Properties of polypropylene fiber reinforced concrete using recycled aggregates," *Construction and Building Materials*, vol. 98, pp. 620–630, 2015.

[19] K. C. Xu, B. Fu, M. C. Chen, and C. L. Huang, "On the chloride lonpermeability of lepidolitne slag concrete under pressure," *Journal of Experimental Mechanics*, vol. 31, no. 6, pp. 819–826, 2016.

[20] W. Wang, W. Jin, and W. Zhe, "Chloride diffusion coefficient of recycled aggregate concrete under compressive loading," *Materials and Structures*, vol. 49, no. 11, pp. 4729–4736, 2016.

[21] S. Parviz, A. Fadhel, C. Habibur, A. Nossoni, and G. Sarwar, "Cement bonded straw board subjected to accelerated processing," *Cement and Concrete Composites*, vol. 26, no. 7, pp. 797–802, 2003.

[22] J. X. Yao, B. M. Zhou, F. G. Wang, and X. D. Xu, "Experimental study on thermal insulation performance of straw concrete," *New building materials*, vol. 44, no. 3, pp. 86–89, 2017.

[23] H. Q. Sun, B. Xu, and C. F. Yuan, "Research on chlorede ion permeability of polypropylene fiber reinforced concrete after high temperature," *Concrete*, no. 6, pp. 31–34, 2016.

[24] A. N. Noumowe, R. Siddique, and G. Debicki, "Ermeability of high performance concrete subjected to elevate temperature," *Construction and Building Materials*, vol. 23, no. 5, pp. 1855–1861, 2009.

[25] G. Mazzucco, C. E. Majorana, and V. A. Salomoni, "Numerical simulation of polypropylene fibers in concrete materials under fire conditions," *Computers and tructures*, vol. 154, pp. 17–28, 2015.

[26] P. Lura and G. P. Terrasi, "Reduction of fire spalling inhigh-performance concrete by means of superabsorbent polymers and polypropylene fibers," *Cement and Concrete Composites*, vol. 49, pp. 36–42, 2014.

[27] M. Zeiml, D. Leithner, R. Lackner, and H. Mang, "How do polypropylene fibers improve the spalling behavior of in-situ concrete," *Cement and Concrete Research*, vol. 36, no. 5, pp. 929–942, 2006.

[28] J. Bosnjak, J. Ozbolt, and R. Hahn, "Permeability measurement on high strength concrete without and with polypropylene fibers at elevated temperatures using a new test setup," *Cement and Concrete Research*, vol. 53, pp. 104–111, 2013.

[29] X. P. Yao, Y. Han, and L. Shen, "Experimental study on compressive strength and air permeability of polypropylene fiber reinforced concrete after elevated temperature," *Concrete*, vol. 12, 2020.

[30] B. Hu, E. J. Wei, J. Li, X. Zhu, K. Y. Tian, and K. Cui, "Nonlinear creep model based on shear creep test of granite," *Geomechanics and Engineering*, vol. 27, no. 5, pp. 527–535, 2021.

[31] P. Kalifa, G. Chene, and C. Galle, "High-temperature behaviour of HPC with polypropylene fibres: from spalling to microstructure," *Cement and Concrete Research*, vol. 31, no. 10, pp. 1487–1499, 2001.

[32] G. A. Khoury, "Polypropylene fibres in heated concrete.Part 2: Pressure relief mechanisms and modelling criteria," *Magazine of Concrete Research*, vol. 60, no. 3, pp. 189–204, 2008.

[33] P. K. Mehta and P. J. M. Monteiro, *Concrete:microstructure,proper-ties,and Materials*, McGraw-Hill, New York, 2006.

[34] B. Bai, Q. Nie, Y. Zhang, X. L. Wang, and W. Hu, "Cotransport of heavy metals and SiO_2 particles at different temperatures by seepage," *Journal of Hydrology*, vol. 597, Article ID 125771, 2021.

[35] K. Y. Kim, T. S. Yun, and K. P. Park, "Evaluation of pore structures and cracking in cement paste exposed to elevated temperatures by X-ray computed tomography," *Cement and Concrete Research*, vol. 50, pp. 34–40, 2013.

[36] G. Wang, C. Zhang, B. Zhang, Q. Li, and Z. Shui, "Study on the high-temperature behavior and rehydration characteristics of hardened cement paste," *Fire And Materials*, vol. 36, 2014.

[37] V. Vydra, F. Vodák, O. Kapicková, and S. Hošková, "Effect of temperatureon porosity of concrete for nuclear-safety structures," *Cement and Concrete Research*, vol. 31, no. 7, pp. 1023–1026, 2001.

[38] G. Ye, X. Liu, G. D. Schutter, L. Taerwe, and P. Vandevelde, "Phase distribution and microstructural changes of self-compacting cement paste at elevated temperature," *Cement and Concrete Research*, vol. 37, no. 6, pp. 978–987, 2007.

[39] K. Y. Tian, W. D. Gong, E. J. Wei et al., "Gas pressure relief-permeability Increase effect comparative analysis about hydraulic disturbance to soft coal seam and its sandstone roof," *Journal of China Coal Society*, vol. 46, no. 6, pp. 1888–1897, 2021.

[40] I. N. Yadav and K. B. Thapa, "Fatigue damage model of concrete materials," *Theoretical and Applied Fracture Mechanics*, vol. 108, pp. 195–230, 2020.

[41] B. W. Liu, G. Peng, X. L. Ma, and J. H. XIE, "Dynamic damage properties of concrete subjected to cyclic loading and unloading with different lateral stresses," *Journal of Yangtze River Scientific Research Institute*, vol. 34, pp. 121–125+131, 2017.

[42] D. Y. Ma, J. Liu, and J. L. Li, "Research on see page characteristics of sandstone fracture under JRC, confining pressure and axial pressure," *Journal of Natural Disasters*, vol. 27, no. 6, pp. 109–119, 2018.

[43] P. Soroushian, F. Aouadi, H. Chowdhury, A. Nossoni, and G. Sarwar, "Cement bonded straw board subjected to accelerated processing," *Cement and Concrete Composites*, vol. 26, no. 7, pp. 797–802, 2003.

[44] M. Amin, B. A. Tayeh, and I. S. Agwa, "Investigating the mechanical and microstructure properties of fibre-reinforced lightweight concrete under elevated temperatures," *Case Studies in Construction Materials*, vol. 13, Article ID e00459, 2020.

[45] K. Y. Tian, "Study on technology of hydraulic fracturing relieving pressure and increasing permeability in soft coal seam with hard roof," *Journal of Natural Disasters*, vol. 26, no. 4, pp. 215–220, 2017.

[46] M. X. Jing and X. L. Yuan, "Experimental research on corestress sensitivity of carbonate rock," *Natural Gas Industry*, vol. 20, pp. 114–117, 2002.

[47] Z. Liu, L. H. Zhao, X. B. Wu, G. P. Hu, and Q. Y. Zhou, "Damage model of concrete considering hysteretic effect under cyclic loading," *Advanced Engineering Sciences*, vol. 52, no. 4, pp. 117–123, 2020.